Environmental Pollution 261 (2020) 114175

Contents lists available at ScienceDirect

Environmental Pollution

journal homepage: www.elsevier.com/locate/envpol

Understanding phosphate sorption characteristics of mineral amendments in relation to stabilising high legacy P calcareous soil☆

Bingqian Fan [a], Jiahui Ding [a], Owen Fenton [b], Karen Daly [b], Qing Chen [a, *]

[a] Beijing Key Laboratory of Farmyard Soil Pollution Prevention-control and Remediation, College of Resources and Environmental Sciences, China Agricultural University, Beijing, 100193, China
[b] Teagasc, Environmental Research Centre, Johnstown Castle, Co. Wexford, Ireland

ARTICLE INFO

Article history:
Received 13 September 2019
Received in revised form
6 February 2020
Accepted 10 February 2020
Available online 13 February 2020

Keywords:
Phosphorus legacy soil
Alum
Dolomite
Stabilisation
Sorption-desorption

ABSTRACT

In China, excessive phosphorus (P) application in protected vegetable fields has led to high legacy P stores. Soil amendment with alum or dolomite is one of many best management practices (BMPs) used to reduce P losses in calcareous soils. However, both the kinetics and mechanisms of P sorption and soil available P in amended soils are understudied. Herein, both aspects were looked at under controlled conditions. Firstly, a sorption study which coupled P concentrations with poorly-crystalline Al hydroxides and dolomite was conducted. Results from this batch experiment showed that P sorption on poorly-crystalline Al hydroxides was homogenous and occurred mainly via displacement of inner-sphere hydroxyl (Al—OH) instead of the formation of $AlPO_4$. However, the amount of sorbed P reached maximum sorption of 73.1 mg g^{-1} and did not change with further increase in P concentration. It was observed that P adsorbed onto the dolomite surface at low P concentrations, whereas hydroxyl replacement and uneven cluster precipitation of $Ca_3(PO_4)_2$ occurred at high P concentrations. A second 90 day incubation experiment investigated changes to soil available P and sorption-desorption across variable rates of amendments (0—50 g kg^{-1}). Results showed that alum amendment at a rate of 50 g kg^{-1} decreased soil $CaCl_2$—P and Olsen-P concentrations by 91.9% and 57.8%, respectively. However, Olsen-P increased when the dolomite rates were <20 g kg^{-1}. Phosphorus sorption-desorption of the amended soil showed alum had higher P sorption efficiency than dolomite at low addition rates (<10 g kg^{-1}). However, soil amended with high dolomite rates (>10 g kg^{-1}) could sorb more P in comparison with alum when P concentrations were increased. The P status of the amended soil was closely connected to the P sorption mechanisms on mineral amendments, soil P concentrations and soil properties.

1. Introduction

Global anthropogenic phosphorus (P) loads to freshwater have been increasing and it is estimated that 50% of the total load originates from Asia (Mekonnen and Hoekstra, 2018). In China, it has been shown that legacy P stores of 242 kg P ha^{-1} accumulated in arable soils from 1980 to 2007 (Li et al., 2011) and P losses in dissolved as well as particulate form associated with such stores increased by 10-fold in the same period (Powers et al., 2016). Soil amendment of topsoil in protected vegetable fields (PVF) is seen as one of many BMPs to safeguard against leaching and runoff losses from legacy P stores (Fan et al., 2019). Soil amendments, which have been shown to be promising in the available literature, include low-cost P sorbing materials (PSM) such as clay minerals (kaolinite, montmorillonite, illite and zeolite, etc.) or other minerals (gypsum, goethite, ferrihydrite, hematite, gibbsite, ochre, alum, ferric chloride, lime and dolomite etc.) (Brennan et al., 2011; Cieślik and Konieczka, 2017; Cusack et al., 2018; Fenton et al., 2011; Gérard, 2016; Gustafsson et al., 2012; Gypser et al., 2018; Li et al., 2018; Miyittah et al., 2011).

Alum or alum-based water treatment residuals (WTRs) have been proven to effectively reduce P losses from poultry litter and high P alkaline soil (Anderson et al., 2018; Novak and Watts, 2005; Zhao et al., 2018). A previous study of Huang et al. (2018) suggested that alum reacts with P to form Al—P complexes at a pH > 7 via the first formation of Al hydroxides followed by adsorption of P. Similarly, the recent study of Fan et al. (2019), which used P K-edge X-ray

☆ This paper has been recommended for acceptance by Jörg Rinklebe.
* Corresponding author.
E-mail address: qchen@cau.edu.cn (Q. Chen).

https://doi.org/10.1016/j.envpol.2020.114175
0269-7491/

absorption spectroscopy (XANES) to distinguish P species in the P-enriched alkaline calcareous soil with alum addition, also indicated the formation of poorly-crystalline Al hydroxides. The mechanisms of P sorption on the Al hydroxides depend on P concentrations, pH, ionic strength, and the presence of competing or complexing ions (Arai and Sparks, 2007; Essington, 2015; Wan et al., 2019). During past decades, the investigation of sorption reactions at mineral/water interfaces using approaches ranging from macroscopic to molecular scale contributed to advancements in P pollution control in the soil environment (Li et al., 2013a; Lookman et al., 1994; Wang et al., 2019). Rajan et al. (1974) found that at the water-hydrous alumina interface, P adsorption mainly occurred through the displacement of aquo groups (Al−H_2O) at low P concentrations. Hydroxy groups (Al−OH) on the other hand became the predominant sites of sorption when the P concentration was increased. Also it was speculated that hydroxyl bridges linking Al atoms (Al−OH−Al) would be broken at higher P concentration and that conversion of Al−OH to Al−H_2O was to be expected below the zero point charge (Rajan et al., 1974). The study of Shang et al. (1992) investigated the pH effect on the sorption of P on poorly-crystalline Al hydroxides at pH 4.5–6.5. It was demonstrated that an increase in pH decreases the quantity of aquo groups and thus also decreases the amount of adsorbed P. Lookman et al. (1997) used magic angle spinning (MAS) nuclear magnetic resonance (NMR), which can distinguish surface adsorption and precipitation of P on Al hydroxides based on chemical shifts, to investigate P sorption on amorphous Al hydroxides obtained at pH 7. The reaction product is amorphous octahedral aluminium phosphate. However, Li et al. (2013a) used ^{31}P solid-state NMR spectroscopy and found that the formation of the bidentate binuclear inner-sphere surface complexes on the air-dried γ-AlOOH at pH 6 was the dominant mechanism. Additionally, a batch experiment of P sorption on amorphous $Al(OH)_3$ at pH 6 characterised by Fourier-transform infrared spectra (FTIR) revealed that outer and inner-sphere P sorption occurred while weakly bound outer-sphere complexes can readily desorb (Gypser et al., 2018). Consequently, it can be expected that different Al-adsorbents at different pH and P concentrations can substantially impact P sorption (Wang et al., 2019). Therefore, P sorption mechanisms on water/Al hydroxides across pH and P concentration gradients need further investigation. In addition, the variation in P status after amendment should be investigated (Ippolito et al., 2003; O' Flynn et al., 2018; Zhao et al., 2018). However, the limit of many spectroscopic approaches such as NMR and X-ray diffraction (XRD) is that they are relatively insensitive. The use of comprehensive spectroscopic techniques such as XRD, FTIR, NMR and scanning electron microscopy (SEM) offers some new possibilities in terms of remediating agricultural soils with high accumulations of P when combined with traditional extraction techniques.

It is widely accepted that P adsorption and precipitation are closely related to Fe/Al and Ca/Mg (Arai and Sparks, 2007). The low-cost Ca/Mg material dolomite shows potential as a soil amendment in PVF as it is cheap and also available to farmers in China (Li et al., 2018; Yuan et al., 2015). One of the advantages of Ca/Mg materials is that they prevent P losses whilst maintaining plant available P since Ca/Mg minerals are relatively inefficient at stabilising P over short period when compared to Fe/Al minerals (Gérard, 2016; Rydin, 2000; Zak et al., 2004). However, P sorbed on the Ca/Mg minerals can be turned to stable Ca/Mg–P such as apatite after a long time (Helfenstein et al., 2018). A kinetic study of the P sorption on dolomite, characterised by XRD spectra, indicated that P removal was mainly controlled by precipitation at P concentrations of 0–50 mg kg^{-1} (Eslamian et al., 2018). Wan et al. (2016) used the FTIR, XRD, SEM, and NMR approaches to demonstrate that crystalline hydroxylapatite precipitates could be formed on the smooth cleavage of calcite at pH 8.5 after interacting with P. This study indicated the interaction of P with calcite involved dissolution of calcite and re-precipitation of previously dissolved Ca^{2+}. Fan et al. (2019) found a significant increase of soil exchangeable Mg^{2+} after dolomite was added to the calcareous soil. In addition, Mg in dolomite could compete with Ca to form $Mg_3(PO_4)_2$ Li et al. (2018). Cao and Harris (2007) also reported Mg inhibited the formation of stable Ca−P when Ca was substituted by Mg. In addition, when dolomite is added to soil, the associated increase of soil pH could affect soil available P, which in turn affects P sorption-desorption dynamics. Murrmann and Peech (1969) reported P in the calcareous soils could be released at higher pH (>7.5) due to the occupation of the Ca^{2+} by −OH. However, it is also noted that P solubility can decrease again at very high pH (>8–9) due to Ca–P mineral precipitation, such as octacalcium phosphate (OCP) and HAP (Eslamian et al., 2018). A more thorough understanding of how P sorption occurs on dolomite and dolomite amended soil will enable a balance to be struck between agronomic (target yields achieved) and environmental (minimise leached losses of P) goals (Hosni and Srasra, 2010; Yuan et al., 2015).

The objectives of the present series of experiments were a) to use a combination of techniques to examine the kinetics and mechanisms of P sorption on poorly-crystalline Al hydroxides and dolomite minerals and b) to expand P sorption characteristics on minerals to soils amended with alum and dolomite in an attempt to elucidate variation in soil available P and P sorption-desorption.

2. Materials and methods

2.1. Mineral amendments

The mineral amendments used in the present study were commercial-grade alum (≥99.8% $KAl(SO_4)_2$ in dry basis) with pH 2.83 (w/v 1: 2.5) and dolomite (containing 22.4% Ca and 13.4% Mg) with pH 9.88 (w/v 1: 2.5). The specific surface area (S_{BEF}) of the sieved alum and dolomite were 0.46 and 2.83 $m^2\ g^{-1}$, respectively, which were determined using a Quantachrome instrument at 77 K with nitrogen adsorptive medium. Before incorporation into the homogenised soil, the amendments were dried and sieved through nylon mesh with 100 mesh number.

2.2. Macroscopic P sorption

To examine P sorption mechanisms on Al hydroxides, a poorly-crystalline Al hydroxide was obtained following the method of Sujana et al. (2009), whereby 1 mol L^{-1} KOH was added to 0.1 mol L^{-1} $KAl(SO_4)_2 \cdot 12\ H_2O$ at pH 7.2. The developed precipitate was washed 2 times with hot water at 60 °C and centrifuged for 15 min at 4000 rpm. The washed precipitate was dried at 60 °C and ground into a powder. The XRD analysis showed that the precipitate was poorly-crystalline (Supporting Information, Fig. S1). Dolomite was sourced from the Cheng De mineral processing plant (Hebei province, China). The formation of dolomite in this district was influenced by serpentine. $CaCO_3$ and $Mg(OH)_2$ were detected in dolomite by XRD analysis (Supporting Information, Fig. S2).

All P sorption tests were conducted in triplicate using 0.1 g of poorly-crystalline Al hydroxides or 0.5 g dolomite in 40 ml P solution with varying concentrations of phosphate. Specifically this was 10, 50, 100, 200, 400 and 500 mg P L^{-1} for poorly-crystalline Al hydroxides and 10, 20, 40, 60, 80, 100, 160, 240, 320, 400 and 500 mg P L^{-1} for dolomite. The pH of the suspension was controlled at pH 6.5 for poorly-crystalline Al hydroxides and at pH 8 for dolomite using 0.05 M HCl and NaOH. Each test was placed in an end over end shaker for 24 h, centrifuged at 3500 rpm and the supernatant was filtered (0.45 μm) and analysed for P concentration. The remaining solid matter was dried at 60 °C.

2.3. Microscopic characterisation of P sorption

In order to investigate the variation in structure, functional groups, surface morphology and sorption types of poorly-crystalline Al hydroxides and dolomite before and after P sorption, XRD, attenuated total reflectance Fourier-transform infrared spectra (ATR-FTIR) between the wavenumbers of 500–4000 cm^{-1}, SEM images and solid-state ^{27}Al and ^{31}P NMR were acquired. The variation of the mineral structure was determined with a D/max-2500/PC (Rigaku, Japan) X-ray diffractometer. The changes of the functional groups were identified using a V70 (Bruker, Germany) Fourier transform infrared. The surface morphology was evaluated using a SU8010 (Hitachi, Japan) SEM equipped with an energy dispersive X-ray spectrometer (EDS). Solid-state ^{27}Al and ^{31}P NMR single-pulse MAS (SP/MAS) NMR spectra were collected on a 600 MHz JNM-ECZ600R spectrometer (JEOL, Japan). The ^{27}Al and ^{31}P SP/MAS NMR spectra were collected at operating frequencies of 156 MHz and 242.8 MHz respectively, with samples contained in 3.2 mm (tube diameter) ZrO_2 rotors at a spining rate of 12 KHz. The relaxation delay was 5s for ^{27}Al and ^{31}P. The ^{31}P chemical shifts of the P adsorbed on poorly-crystalline Al hydroxides were reported relative to a standard $AlPO_4$ sample purchased from Sigma-Aldrich.

2.4. P transformation in the incubated soil amended with alum and dolomite

The intensively cultivated soil was selected from one of the typical PVF located in Fangshan district (39.38°N, 116.10°E), Beijing, China, with a typical continental monsoon climate. Annual mean temperature is 11.6 °C and precipitation is 603 mm. The site has a 5-year rotation of tomato and leafy vegetables and received high application rates of chicken manure (150 m^3 ha^{-1} yr^{-1}) and urea (750 kg ha^{-1} yr^{-1}). Soil samples were collected in April 2017. The topsoil was extracted from 0 to 20 cm depth. After extraction, the soil was air-dried and coarse rocks and plant residue were removed before it was sieved to 2 mm and homogenised. The soil is classified as Calcaric Cambisol (US taxonomy) or Brown soil (Chinese taxonomy) (Brady and Weil, 2019). It has a silty loam texture (sand 27.1%, silt 57.8%, clay 15.3%) with a pH of 7.56, 226 mg kg^{-1} Olsen-P, 11.4 g kg^{-1} organic carbon (OC), 414 mg kg^{-1} Mehlich3-P and 1.36 g kg^{-1} total P. For the criteria of soil Olsen-P, the proposed optimum available soil P level for vegetable fields is 60–90 mg kg^{-1} (Liang et al., 2013).

For each 0.7-L cylindrical incubation container (80 mm diameter × 88 mm height, n = 39) dried and sieved alum or dolomite were mixed with 300 g of the soil (bulk density of 1.32 g kg^{-1}). The following treatments with three replicates of each were assembled: 0 (soil only), 0.5, 1, 5, 10, 20, and 50 g kg^{-1}. Deionised water was added to each container to achieve ~70% field water holding capacity. The containers were covered with parafilm and perforated for air circulation and were then placed in a dark temperature-controlled (25 °C) incubation chamber. Soil treatments were removed from the containers after a 90 d incubation period, air dried and sieved again through 2 mm for analysis. Soil

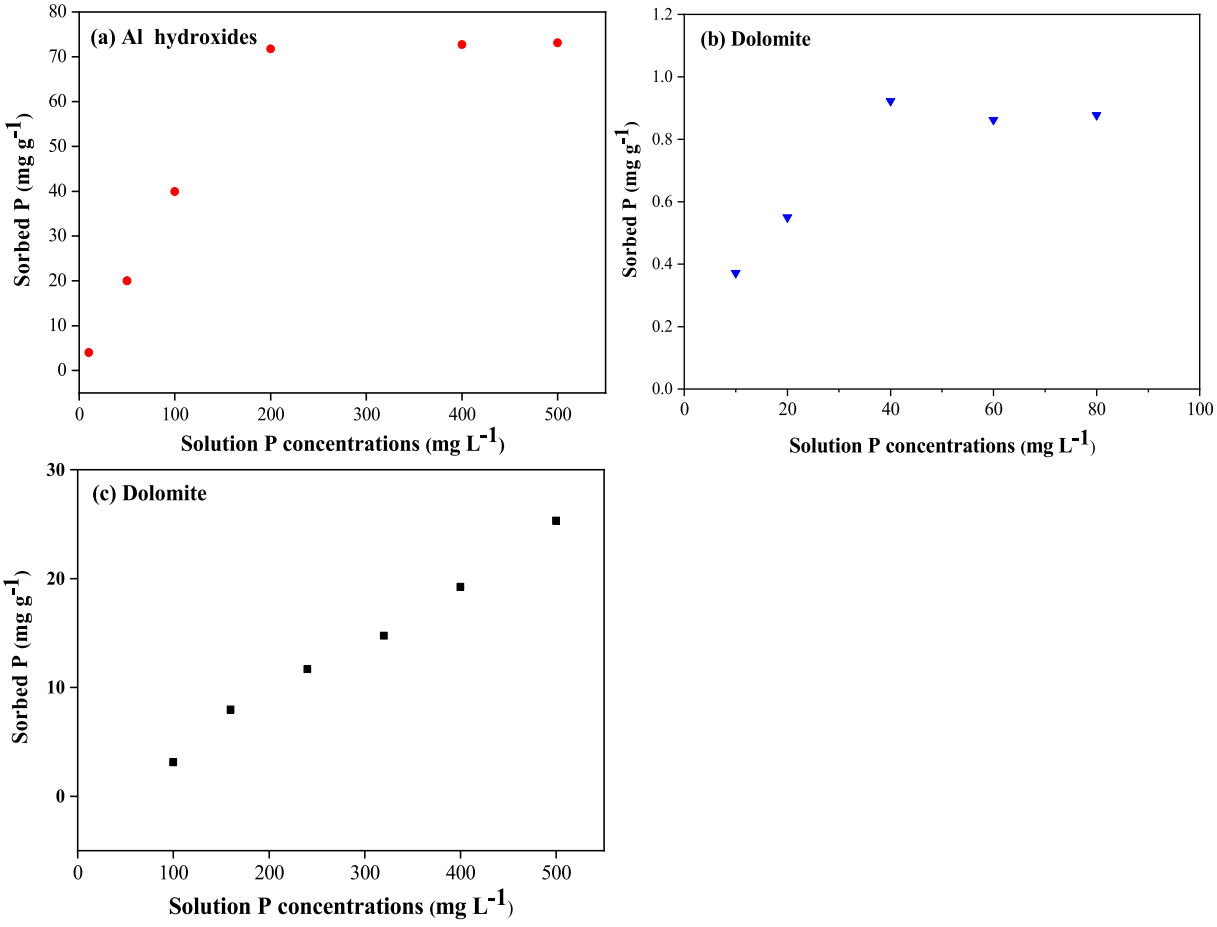

Fig. 1. Effect of initial P concentration on P sorption on (a) poorly-crystalline Al hydroxides and (b and c) dolomite. 0.1 g poorly-crystalline Al hydroxides in 40 ml solution with varying concentrations of P at 10, 50, 100, 200, 400 and 500 mg L^{-1} and 0.5 g dolomite in 40 ml P solution with varying concentrations of P at 10, 20, 40, 60, 80, 100, 160, 240, 320, 400 and 500 mg L^{-1} were conducted. Data are the means of three replicates.

pH was measured in distilled water with soil/solution ratio of 1:2.5 using pH meter (MP522 version 3, SANXIN, China). Soil $CaCl_2$–P and Olsen-P were determined using 0.01 M $CaCl_2$ (soil/solution ratio of 1:5) and 0.5 M $NaHCO_3$ (soil/solution ratio of 1:20), respectively (Olsen, 1954; Schofield, 1955). Phosphorus concentrations in extracts were measured by colorimetric analysis (Murphy and Riley, 1962). In order to examine sequential P fractionation, soil samples from all treatments were subjected to the method initially proposed by Jiang and Gu (1989) and later modified by Adhami et al. (2006) and Audette et al. (2016). In the modified method, the P fraction was extracted as follows: 1.25 g of soil was weighed into a 50 ml polyethylene centrifuge tube. As the first extractant, 25 ml $NaHCO_3$ at pH 7.5 were added to the centrifuge tube. After shaking for 1 h, centrifugation was used at 4000 rpm for 8 min and the supernatant was then removed and filtered. This extraction procedure was repeated sequentially with seven types of extractants (0.25 M $NaHCO_3$, 0.5 M CH_3COONH_4, 1 M $MgCl_2$, 0.5 M NH_4F, 0.1 M NaOH-0.5 M Na_2CO_3, 0.3 M $Na_3C_6H_5O_7$–$Na_2S_2O_4$-0.5 M NaOH and 0.5 M H_2SO_4) using the required shaking/standing time (Audette et al., 2016). It was noted that the extraction with 1 M $MgCl_2$ in the third step of the modified method did not extract P forms but instead recovered P that was re-adsorbed to the unattached substrates (Audette et al., 2016). Therefore, the six P fractions were extracted as follows: Ca_2–P, Ca_8–P, Al–P, Fe–P, Occluded-P and Ca_{10}–P.

2.5. P sorption-desorption in the soil amended with alum and dolomite

To examine the P sorption capacity of the amended soils, P sorption isotherms were constructed using the method of Pautler and Sims (2000). For this purpose, 2 g of soil at the end of 90 d incubation in duplicate were weighed in 50-ml centrifuge tubes. These soil samples were combined with eight 30 ml solutions (0, 1, 5, 10, 15, 20, 25, 50 mg P L^{-1}) made up from a KH_2PO_4 stock solution (500 mg P L^{-1}) with 0.01 M $CaCl_2$ as the background solution. Two

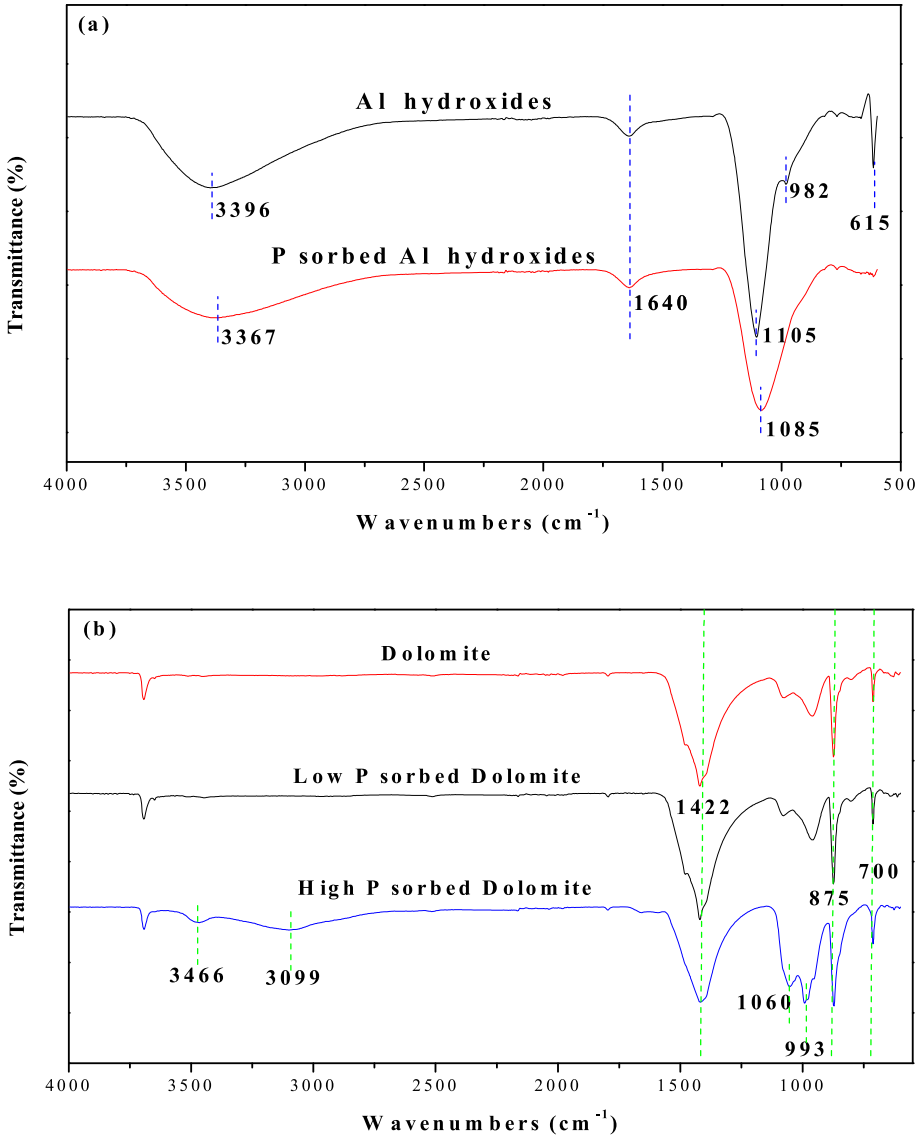

Fig. 2. Attenuated total reflectance Fourier-transform infrared (ATR-FTIR) spectra in the 500-4000 cm^{-1} region of (a) poorly-crystalline Al hydroxides (black line) and P sorbed poorly-crystalline Al hydroxides (red line) and (b) dolomite (red line), low P sorbed dolomite (black line) and high P sorbed dolomite (blue line). P sorbed poorly-crystalline Al hydroxides is the mixture of all the dried isotherm samples after P sorption. Low P sorbed dolomite and high P sorbed dolomite is the mixture of dried isotherm samples after 10–80 and 100–500 mg L^{-1} P solution was sorbed. (For interpretation of the references to color in this figure legend, the reader is referred to the Web version of this article.)

drops of toluene were added to restrict microbial activity. The suspensions were shaken (25 °C for 24 h), centrifuged and filtered (Whatman No. 42) and the concentration of P in the solution was measured by colorimetric analysis (Murphy and Riley, 1962). The P adsorbed to the soil was calculated as the difference between initial P concentration and final P concentration measured at equilibrium. Afterwards, a P desorption experiment was performed. Each 50 ml tube was filled with 30 mL of 0.01 mol L^{-1} $CaCl_2$ solution. The tubes were shaken for 24 h. After shaking, the suspensions were centrifuged at 4000 rpm for 8 min and then filtered through a Whatman filter No. 42 paper. The final P concentration of the supernatant was measured using the colorimetric method (Murphy and Riley, 1962). The amount of P desorbed was determined by subtracting the residual P in tubes from the measured P after the P desorption experiment.

2.6. Statistical analysis

The Jade (5.0) software equipped with the PDF 2004 database was used to analyse the XRD spectra. All statistical data were analysed using Microsoft Excel 2016 and figures were made by Origin 8.0. Analysis of variance (ANOVA) was used to determine the statistical significance of the treatment effects based on randomised complete block design. Multiple comparisons of mean values of $CaCl_2$–P, Olsen-P, pH, P contents in soil P fraction were performed using the Fisher's least significant difference (LSD, $P < 0.05$) among different treatments. IBM SPSS 19.0 software was used for all statistical tests.

3. Results

3.1. P sorption on poorly-crystalline Al hydroxides

Sorption isotherms are presented in Fig. 1a as the plot of initial P concentration *vs.* P sorbed on poorly-crystalline Al hydroxides. The amounts of P sorbed at equilibrium increased from 4.0 to 73.1 mg g^{-1} with an increase of initial P concentration ranging from 10 to 500 mg L^{-1} (Fig. 1a). It showed that >99% of P was sorbed when the initial P concentration was <100 mg L^{-1}. However, the amount of sorbed P nearly saturated when the initial P concentration increased up to 200 mg L^{-1}, while the equilibrium P concentration maintained approximately 180 mg L^{-1} when the initial P concentration increased from 200 mg L^{-1} to 500 mg L^{-1} (Fig. 1a). After P was sorbed on the poorly-crystalline Al hydroxides, the SEM-EDS images showed that P was sorbed evenly (Supplementary Information, Fig. S3c). Results of the ATR-FTIR showed that the intensities of the P–O stretching band at 1085 cm^{-1} (Krumina et al., 2016) increased while the –OH stretching vibrations bands at 982 and 3396 cm^{-1} decreased (Fig. 2a). The band of the –OH stretching vibrations at around 3400 cm^{-1} can be assigned to out-sphere –OH groups (Egorova and Lamberov, 2015) while 982 cm^{-1} was described as inner-sphere deformation vibrations of OH-groups (Ruan et al., 2001) or bending vibrations of weakly interacting hydroxyl groups (Kolesova and Ryskin, 1959). In addition, the deformation vibration of the H_2O group at 1640 cm^{-1}, which can be assigned to the bending mode of molecular H_2O-groups associated with Al (Al–H_2O) (Myronyuk et al., 2016), increased after P sorption (Fig. 2a). However, the XRD spectrum did not detect the formation of $AlPO_4$. This was confirmed by the ^{27}Al NMR spectra which detected a negligible differential of ^{27}Al chemical shift (δ_{Al}) (Fig. 3a) for the poorly-crystalline Al hydroxides before and after P sorption. In addition, the ^{31}P NMR showed that the ^{31}P chemical shift (δ_p) of the $AlPO_4$ at $\delta_p = -49.59$ was not detected on P sorbed poorly-crystalline Al hydroxides (Fig. 3b).

3.2. P sorption on dolomite

The amounts of P sorbed on dolomite increased from 0.37 to 0.97 mg g^{-1} with the initial P concentration ranging from 10 to 80 mg L^{-1} (Fig. 1b). However, the sorbed P increased significantly from 3.1 to 25.3 mg g^{-1} when the initial P concentrations were increased from 100 to 500 mg L^{-1} (Fig. 1c). Examination of the graphical isotherm data strongly suggested a multiple steps or mechanisms sorption process on the dolomite as proven by the noticeable change of the P sorbed amounts (Fig. 1b–c). Hence, the dried isotherm samples were mixed with the initial P concentrations ranging from 0 to 80 mg L^{-1} and from 100 to 500 mg L^{-1}, which were labelled low P sorbed dolomite and high P sorbed dolomite respectively.

The ATR-FTIR spectrum of dolomite showed a sharp absorbance band at 1422 and 875 cm^{-1} due to C–O stretching vibrations of CO_3^{2-} (Fig. 2b) (Gunasekaran et al., 2006). For the low P sorbed dolomite, a negligible increase absorbance band at 1080 cm^{-1} was found when compared with the dolomite sample. However, the

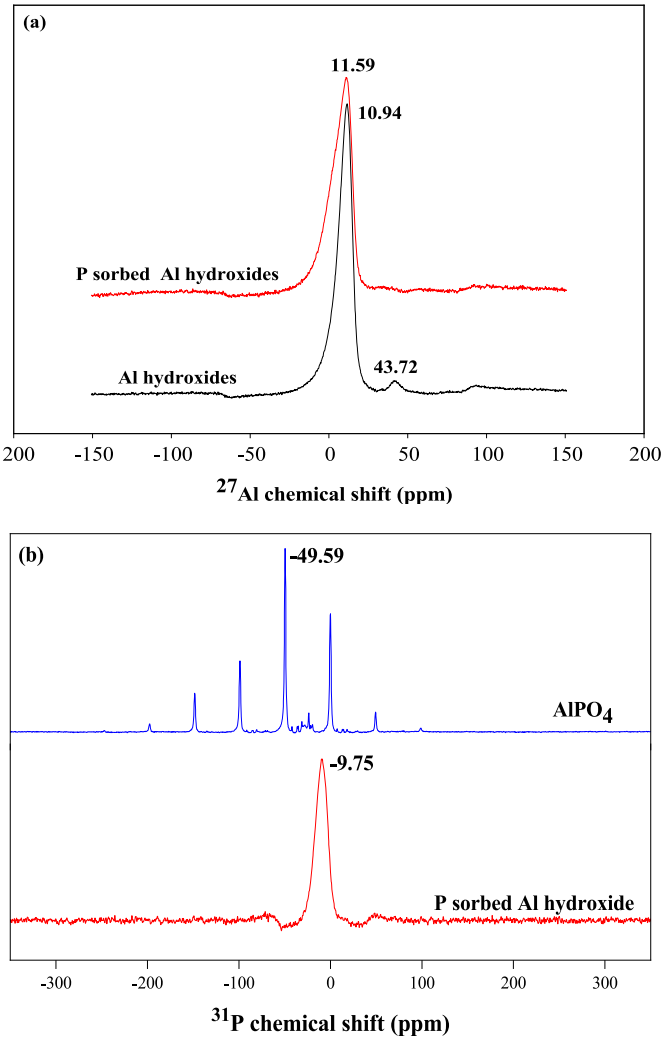

Fig. 3. Solid-state (a) ^{27}Al NMR of poorly-crystalline Al hydroxides (black line) and P sorbed poorly-crystalline Al (red line), and (b) ^{31}P NMR of the P sorbed poorly-crystalline Al (red line) and $AlPO_4$ (blue Line). The Al chemical shift at $\delta_{Al} = 43.72$ ppm assigned to the impurity of K_2SO_4 in poorly-crystalline Al hydroxides. P sorbed poorly-crystalline Al hydroxides is the mixture of all the dried isotherm samples after P sorption. (For interpretation of the references to color in this figure legend, the reader is referred to the Web version of this article.)

relative intensity of the new absorbance bands at 1060 and 993 cm^{-1} which was assigned to the Mg–P phases (Zhou et al., 2011) and C–O–P vibrations (Ganesan and Epple, 2008) were detected in the high P sorbed dolomite. Also, the –OH stretching vibration was found at around 3466 cm^{-1} (Fig. 2b). The $Ca_3(PO_4)_2$ was detected in the high P sorbed dolomite (Supplementary Information, Fig. S2) and the SEM-EDS images also showed uneven clusters of P precipitation around the $CaCO_3$ (Supplementary Information, Fig. S4 c-d, and Figs. S5c–d). The ^{31}P NMR spectra of P sorption on dolomite showed a ^{31} P chemical shift (δ_P) at $\delta_P = 3.24$ ppm for low P sorbed dolomite and at $\delta_P = 5.61$ ppm for high P sorbed dolomite. The $\delta_P = 5.61$ ppm resembled the spectra of calcium phosphate previously reported by Hinedi et al. (1992).

3.3. Change in soil available P with alum and dolomite addition

Soil $CaCl_2$–P and Olsen-P significantly decreased with increasing rates of alum. It was found that alum addition rate from 0.5 to 50 g kg^{-1} of soil dry weight, reduced soil $CaCl_2$–P by 3.9–91.9% and soil Olsen-P by 9.2 and 57.8% relative to the control treatment after the 90 d incubation (Fig. 5). The results of the soil P fractionation suggested that P desorbed from Ca minerals and adsorbed to Al hydroxides (Table 1). Adding 0.5–50.0 g kg^{-1} of alum caused a soil Ca_2–P reduction between 3.3 and 80.5 mg kg^{-1} and soil Ca_8–P reduction between 15.6 and 306.8 mg kg^{-1}. A corresponding increment of Al–P between 14.9 and 394 mg kg^{-1} was found in the soil amended with different rates of alum. However, there were no significant differences among alum treatments and the control treatment with respect to the Fe–P, occluded P (O–P) and Ca_{10}–P.

Compared with the untreated soil after 90 d incubation, mixing dolomite in the range of 0.5, 1, 5, 10, 20 and 50 g kg^{-1} of soil dry weight, reduced soil $CaCl_2$–P by 2.6, 5.2, 39.7, 53.6, 65.8 and 70.5%, respectively (Fig. 5). Although higher rates such as 50 g kg^{-1} were more capable of reducing soil $CaCl_2$–P, there was no significant reduction noted between the rate of 20 and 50 g kg^{-1}. However, in addition to a dolomite amendment rate of 50 g kg^{-1} reduced soil Olsen-P by 3.1%, dolomite rates of 0.5, 1, 5, 10 and 20 g kg^{-1} significantly increased the soil Olsen-P values by 6.8, 9.4, 14.4, 19.0, 19.2%, respectively (Fig. 5). Also, compared with the control treatment, the dolomite rates between 0.5 and 50 g kg^{-1} resulted in an increase in Ca_2–P contents between 2.2% and 28.0% and a reduction of Ca_8–P contents between 8.1% and 25.8%.

3.4. P sorption-desorption isotherms of the amended soil

The P sorption isotherms for all soil treatments were presented in Table 2. When the initial P concentrations were increased from 0 to 50 mg L^{-1}, the amounts of sorbed P in the control treatment changed from –36 to 143 mg kg^{-1}. The P sorbed amounts increased in all soil treatments amended with 0.5–50 g kg^{-1} of alum (Table 2). Soil treatments with 5, 10 20 and 50 g kg^{-1} of dolomite added showed P sorbed amounts of –21 to 232 mg kg^{-1}, -11 to 522 mg kg^{-1}, -6 to 597 mg kg^{-1} and -3 to 706 mg kg^{-1}, respectively. Low dolomite addition rates (0.5 and 1 g kg^{-1}) on the other hand caused a reduction of the P sorbed amounts (Table 2).

The P desorbed amounts increased from 16.2 to 68.8 mg kg^{-1} in the control treatment with the P sorbed amounts varying from –36 to 143 mg kg^{-1} (Table 2). The P desorbed amounts in soil treatments were closely linked to the alum or dolomite rates (Table 2). Generally, P release (P desorbed percentage of P sorbed) decreased when the alum rates and P concentrations used in the sorption experiments were increased (Table 2). For the soil treatments amended with dolomite, it was noted that the P release increased when the dolomite rates were raised from 0.5 to 1 mg kg^{-1}, whilst a rapid decline of P release was found when the dolomite rates were raised from 5 to 50 g kg^{-1}.

4. Discussion

4.1. Mechanism of P sorption on poorly-crystalline Al hydroxides

In the present study the poorly-crystalline Al hydroxides at pH 6.5 had higher P sorption amounts (Fig. 1a) than many other reported Al-sorbents; such as γ-alumina (11.2 mg g^{-1}), boehmite (7.87 mg g^{-1}) (Li et al., 2013a) and amorphous $Al(OH)_3$ produced at pH 6 (23.9 mg g^{-1}) (Gypser et al., 2018). Notably, the amount of sorbed P on this poorly-crystalline Al hydroxides was less than that on the amorphous $Al(OH)_3$ obtained at pH 4 in the study of Wang et al. (2019), where P sorption maxima reached up to 143 mg g^{-1}.

Table 1
Contents of different fractions of inorganic P (P_i) and organic P in the calcareous soils by adding different rates of alum and dolomite after 90 d incubation.

Treatment	Ca_2–P[a]	Ca_8–P	Al–P	Fe–P	O–P	Ca_{10}–P	Organic P[c]
	(mg kg^{-1})						
Added amount of alum (g kg^{-1})							
0 (Control)	116.9A[b]	346.8A	98.1F	38.2A	143.5A	366.4BC	214.8A
0.5	117.8A	331.2AB	113.0E	36.7A	151.9A	370.4BC	186.0A
1	113.6A	315.2B	115.7E	35.8A	153.8A	353.0C	217.8A
5	95.4B	265.5C	200.6D	40.2A	170.5A	372.7B	187.1A
10	79.2C	198.5D	273.2C	38.3A	145.4A	365.2BC	210.3A
20	58.8D	110.0E	405.9B	36.4A	142.6A	378.2BC	198.3A
50	36.4E	40.0F	492.1A	41.1A	162.1A	392.4A	189.6A
Added amount of dolomite (g kg^{-1})							
0 (Control)	116.9e	346.8a	98.1ab	38.2a	143.5a	366.4a	214.8a
0.5	119.5de	364.5a	113.9a	37.5a	145.4a	357.3a	203.5a
1	124.7d	351.9a	106.7ab	39.7a	151.0a	357.0a	210.3a
5	134.7c	318.6b	93.1b	40.1a	147.3a	349.9a	196.3a
10	141.2b	310.6b	103.5ab	35.6a	164.0a	368.4a	213.5a
20	141.9b	295.0b	113.0ab	35.8a	123.1a	370.4a	233.8a
50	149.7a	257.5c	116.2a	39.4a	134.9a	364.4a	210.9a

[a] Ca_2–P, Ca_8–P, Al–P, Fe–P, occlude-P (O–P) and Ca_{10}–P was fractioned with modified Jiang and Gu method and were extracted with 25 ml 0.25 M $NaHCO_3$, 0.5 M NH_4AOc, 0.5 M NH_4F, 0.1 M NaOH-0.5 M Na_2CO_3, 0.3 M $Na_3C_6H_5O_7$–$Na_2S_2O_4$ (1 g)-0.5 M NaOH and 0.5 M H_2SO_4 respectively.
[b] Capital letter means the differences among the control and alum treatments, the small letter means the differences among the control and dolomite treatments. Data are the means of three replicates. Different letters in different treatments are significant at $P < 0.05$.
[c] Organic P was determined by the ignition method.

Previous studies of Wang et al. (2019) and Shang et al. (1992) reported that the decline of the pH increased the P sorbed amounts as the formation of the $AlPO_4$. However, the ^{27}Al NMR spectra showed a negligible differential of ^{27}Al chemical shift (δ_{Al}) for the poorly-crystalline Al hydroxides before and after P sorption (Fig. 3a). Also, ^{31}P NMR showed the ^{31}P chemical shift (δ_p) of the $AlPO_4$ at $\delta_p = -49.59$ was not detected on P sorbed poorly-crystalline Al hydroxides (Fig. 3b). This study confirmed that $AlPO_4$ precipitation did not occur at pH 6.5, which was consistent with the results of Li et al. (2013a) and Wang et al. (2019). Makris et al. (2004) also deduced from SEM-EDS elemental maps that homogenous P distribution at the surface of Al-WTRs represented sorption, whereas no evidence was found for precipitation, in accordance with the XRD (Supplementary Information, Fig. S1) and SEM-EDS results found in this study (Supplementary Information, Fig. S3).

Therefore, the P–O stretching band at 1085 cm^{-1}, the decrease of the vibration bands at 982 and 3400 cm^{-1} in the ATR-FTIR spectra (Fig. 2a) indicated the P sorption on poorly-crystalline Al hydroxides through displacement of outer and inner-sphere Al–OH groups. The study of Li et al. (2013b) reported the ^{31}P NMR chemical shifts of outer-sphere and inner-sphere precipitation were -10-0 ppm and 0–10 ppm. Since the ^{31}P chemical shift of the P sorbed poorly-crystalline Al hydroxides was at δ_p = -9.75 ppm in this study (Fig. 3b), it was identified that the increase of P–O stretching vibration was mainly assigned to P exchanged with inner-sphere –OH groups and corresponding bidentate complexes formed (Li et al., 2013a). Gypser et al. (2018) reported strongly bound inner-sphere complexed P is difficult to release. It was noted that based on the theory of Rajan et al. (1974), the displacement of Al–H_2O groups was prior to the surface –OH groups which led to a decrease in the vibration of the Al–H_2O groups. The opposite result was observed here. It was speculated here that P displaced Al–H_2O groups first, but that new Al–H_2O groups would also form later. These results were in line with Rajan et al. (1974), who speculated that a higher P concentration might split Al–OH–Al groups and form H_2O molecules.

4.2. Mechanism of P sorption on dolomite

The study of Hinedi et al. (1992) showed P sorption amounts on

Table 2
Phosphorus sorbed, desorbed amounts (mg kg^{-1}) and P release (%) (the desorbed P percentage of sorbed P) in the calcareous soils by adding different rates of alum and dolomite after 90 d incubation.

Treatment		P concentrations[a] (mg L^{-1})							
		0	1	5	10	15	20	25	50
Added amount of alum (g kg^{-1})									
0 (Control)	P sorbed	−36.4[b]	−20.1	−0.3	20.5	53.3	69.2	82.6	143.2
	P desorbed[c]	16.2	22.2	28.6	38.0	45.4	50.9	56.2	68.8
	P release	**[d]	**	**	185.0%	85.2%	73.5%	68.0%	48.0%
0.5	P sorbed	−36.6	−22.0	3.8	28.4	58.3	89.7	90.2	165.8
	P desorbed	20.8	22.8	28.4	34.0	45.3	49.1	52.9	73.9
	P release	**	**	**	119.6%	77.7%	54.8%	58.7%	44.6%
1	P sorbed	−28.6	−16.2	10.7	27.6	70.8	88.6	115.0	193.9
	P desorbed	23.4	17.9	31.6	32.9	41.9	44.9	54.4	71.8
	P release	**	**	**	119.2%	59.1%	50.7%	47.3%	37.0%
5	P sorbed	−19.9	−6.8	28.9	66.9	108.0	135.5	169.3	259.8
	P desorbed	12.3	11.2	18.1	25.8	36.0	43.8	49.2	81.3
	P release	**	**	62.8%	38.5%	33.4%	32.3%	29.1%	31.3%
10	P sorbed	−10.9	2.3	48.0	96.7	139.1	172.4	200.5	307.1
	P desorbed	8.8	9.3	15.6	22.4	27.5	37.8	40.3	62.1
	P release	**	**	32.5%	23.1%	19.8%	21.9%	20.1%	20.2%
20	P sorbed	−4.7	9.0	61.4	124.2	181.6	232.4	275.1	450.1
	P desorbed	4.0	4.2	8.0	14.0	21.3	25.3	35.0	49.8
	P release	**	47.1%	13.1%	11.2%	11.7%	10.9%	12.7%	11.1%
50	P sorbed	−1.9	12.5	70.7	142.3	213.5	281.7	349.1	640.5
	P desorbed	0.3	1.9	1.2	5.4	5.4	10.7	16.1	29.9
	P release	**	14.9%	1.7%	3.8%	2.5%	3.8%	4.6%	4.7%
Added amount of dolomite (g kg^{-1})									
0.5	P sorbed	−32.8	−22.4	3.9	32.6	48.8	84.3	77.1	111.8
	P desorbed	19.8	20.0	27.7	36.7	40.9	45.7	48.8	62.5
	P release	**	**	**	112.8%	83.8%	54.2%	63.3%	55.9%
1	P sorbed	−31.5	−21.7	7.7	31.6	53.3	67.8	76.8	105.7
	P desorbed	20.1	22.4	30.0	39.3	43.9	49.2	53.9	70.2
	P release	**	**	**	124.4%	82.5%	72.5%	70.2%	66.4%
5	P sorbed	−20.9	−11.4	28.4	65.4	100.0	157.9	154.7	232.6
	P desorbed	19.3	19.2	27.5	38.7	47.2	55.5	61.2	97.9
	P release	**	**	96.7%	59.3%	47.2%	35.1%	39.5%	42.1%
10	P sorbed	−11.3	1.0	49.7	101.5	156.9	222.7	252.3	522.5
	P desorbed	14.2	15.2	19.0	27.9	38.2	48.8	55.8	83.3
	P release	**	**	38.3%	27.5%	24.3%	21.9%	22.1%	15.9%
20	P sorbed	−6.0	7.1	61.9	127.0	192.6	262.5	313.8	597.5
	P desorbed	7.8	7.6	12.0	17.6	23.1	29.3	34.2	46.2
	P release	**	**	19.4%	13.9%	12.0%	11.2%	10.9%	7.7%
50	P sorbed	−3.2	11.3	69.1	143.4	215.8	291.1	359.1	706.8
	P desorbed	2.9	2.9	3.6	5.2	6.0	7.3	8.4	6.8
	P release	**	25.7%	5.2%	3.6%	2.8%	2.5%	2.3%	1.0%

[a] P concentrations: the initial P concentrations used in the P sorption experiment.
[b] Data are the means of two replicates.
[c] P desorption experiment was conducted with a 30 ml 0.01 M $CaCl_2$ solution after the P sorption experiment.
[d] Data were not shown since soil P desorbed in the P sorption experiment.

calcium carbonate increased with an increase in the added P amounts. However, different results were found for P sorption on dolomite (Fig. 1b–c). Although the XRD and ATR-FTIR spectra did not show differences between the low P sorbed dolomite and dolomite, the SEM-EDS analysis (Supplementary Information, Fig. S5a) and ^{31}P NMR (Fig. 4) of the low P sorbed dolomite sample indicated that P was sorbed on the dolomite surface. Particularly, it was found that more P was sorbed on Mg than Ca in the low P sorbed dolomite (Supplementary Information, Fig. S5b). However, when the P concentration exceeded 100 mg L^{-1}, ATR-FTIR results of the high P sorbed dolomite demonstrated the simultaneous occurrence of P exchange with –OH, defined by the change of the –OH stretching vibration functional groups at 3466 cm^{-1} (Leng et al., 2015), P precipitation evidenced by the bands located at 993 cm^{-1} (Li et al., 2017) and the formation of Mg–P phases confirmed by the new absorbance band at 1060 cm^{-1} (Fig. 2b). The study of Xu et al. (2014) indicated that there is a formation of Mg–P phases at 1060 cm^{-1} when Mg was present, thus providing more –OH functional groups on the surface of calcite, which was in line with the results reported in this study. Wan et al. (2016) investigated phosphate sorption on calcite at pH 8.5 and reported the formation of hydroxylapatite (HAP), which was confirmed by a gradual disappearance of C–O stretching vibrations at 1422 and 875 cm^{-1} as well as the characteristic bands of hydroxylapatite at approximately 961, 1026 and 1126 cm^{-1} due to the P–O stretching vibrations (Ślósarczyk et al., 2005). However, the ATR-FTIR spectra of the high P sorbed dolomite sample in this study did not show the bands of hydroxylapatite, but showed that the absorbance band of C–O stretching vibrations was consistent with the spectrum of dolomite. Cao and Harris (2007) demonstrated that Mg inhibited the precipitation of HAP due to the substitution of Mg^{2+} ions for the Ca^{2+} ions in the HAP structure, whereas it promoted the formation of amorphous calcium phosphate (ACP). A similar result was found in the present study, i.e. XRD spectrum (Supplementary Information, Fig. S2), ^{31}P NMR (Fig. 4) and the SEM-EDS images showed P was precipitated as $Ca_3(PO_4)_2$ around $CaCO_3$ in the high P sorbed dolomite (Supplementary Information, Fig. S5d). Furthermore, SEM-EDS results illustrated that the precipitated P was uneven and cumulated at a certain point along with clusters (Supplementary Information, Figs. S4c–d), which was in line with the results of Bertrand et al. (2001) and Wan et al. (2016) which showed P-cluster on the smooth cleavage surface of calcite.

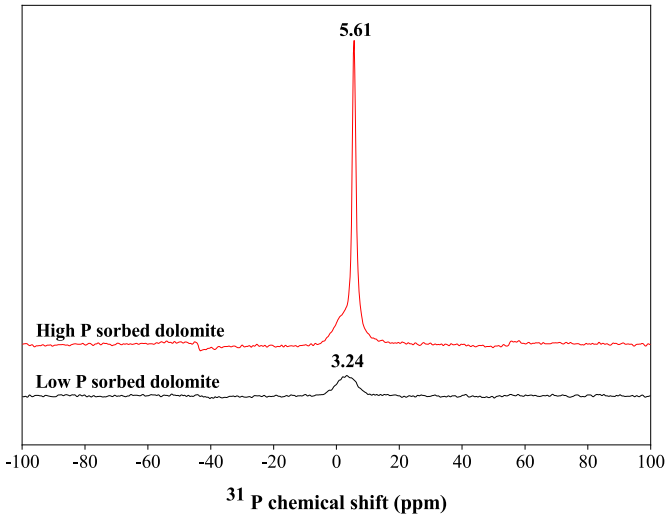

Fig. 4. Solid-state ^{31}P NMR of the low P sorbed dolomite (black line) and high P sorbed dolomite (red line). Low P sorbed dolomite and high P sorbed dolomite is the mixture of dried isotherm samples after 0–80 and 100–500 mg L^{-1} P solution was sorbed. (For interpretation of the references to color in this figure legend, the reader is referred to the Web version of this article.)

4.3. Variation of soil available P

In the natural environment where Al hydroxides or dolomite are present, the fate, transport and bioavailability of P is most likely to be controlled by P stabilisation mechanisms of conditions that are similar to the water/absorbents interface in this study. Results of the incubation soil amended with alum suggested that alum addition caused a decline in soil pH (Table S1), which dissolved the readily soluble Ca–P compounds. This was consistent with the significant increase in soil exchangeable Ca^{2+} (Supplementary Information, Table S1). As the soil pH ranged from 7.2 to 6.8 following 0.5–50 g kg^{-1} of alum addition (Supplementary Information, Table S1), the alum was easily transformed to poorly-crystalline Al hydroxides within the pH range. The production of the Al hydroxides mineral in the present study also indicated the transformation of poorly-crystalline Al hydroxides at pH 7.2 (Supplementary Information, Fig. S1). Based on the theory of P sorption on poorly-crystalline Al hydroxides as discussed above, the P bonding on poorly-crystalline Al hydroxides through replacing of inner-sphere hydroxyl was strong (Fan et al., 2019; Gypser et al., 2018). Therefore, both the soil Ca_2–P and Ca_8–P contents decreased while the Al–P content in the soil P fractionation increased with alum addition (Table 1). Since the Ca_2–P in the high legacy P calcareous soil is the dominant P pool of soil Olsen-P (Fan et al., 2019), a significant decline of Olsen-P was found when alum was added (Fig. 5). However, in the present study soil Olsen-P was still higher than 90 mg kg^{-1} even with 50 g kg^{-1} of alum addition (Fig. 5), which meant plant available P was still abundant while the P loss risk decreased dramatically with alum addition.

For the soil treatments amended with dolomite, the reduction of soil $CaCl_2$–P was due to surface adsorption as the P concentration in the 0.01 M $CaCl_2$ extraction of this calcareous soil was ~2 mg L^{-1}. However, the variation of the Olsen-P was associated with the dual effect of P sorption and the change of the soil pH. Dolomite rates at 0.5–20 g kg^{-1} caused an increase in soil pH ranging from 7.14 to 7.75 (Supplementary Information, Table S1). Consequently, the Ca^{2+} was competed by the OH^- (Supplementary Information, Table S1), which caused the Ca–P release (Li et al., 2018). The results of the soil P fractionation showed an increase in soil Ca_2–P (Table 1) also supported the increase of the soil Olsen-P. However, the released Ca–P could be re-adsorbed onto the dolomite surface, but it was difficult to form stable Ca–P such as hydroxylapatite on the surface of dolomite. This assertion was supported by the significant decrease of the soil $CaCl_2$–P contents and the negligible increase of Ca_{10}–P contents (Table 1), which denoted the stable Ca–P after dolomite addition. Freeman and Rowell (1981) reported the bonding capacity of newly sorbed P on the calcite surface was likely weaker than the phosphate clusters, thus facilitating newly sorbed P to be readily extracted by the Olsen-P extractant. Nevertheless, the formation of the insoluble Ca–P compounds could be found when the soil pH increased continuously (Devau et al., 2011). In this study, soil pH rose up to 8.1 with 50 g kg^{-1} of dolomite added (Supplementary Information, Table S1). Therefore, dolomite rates of 50 g kg^{-1} decreased soil Olsen P.

4.4. Variation of P sorption-desorption

In China, many farmers focus on economic crops such as vegetables believe that high P fertiliser application results in higher crop yields (Zhou et al., 2019). Consequently, heavy manure application such as 10 Mg ha^{-1} year^{-1} in the PVF is quite common although the

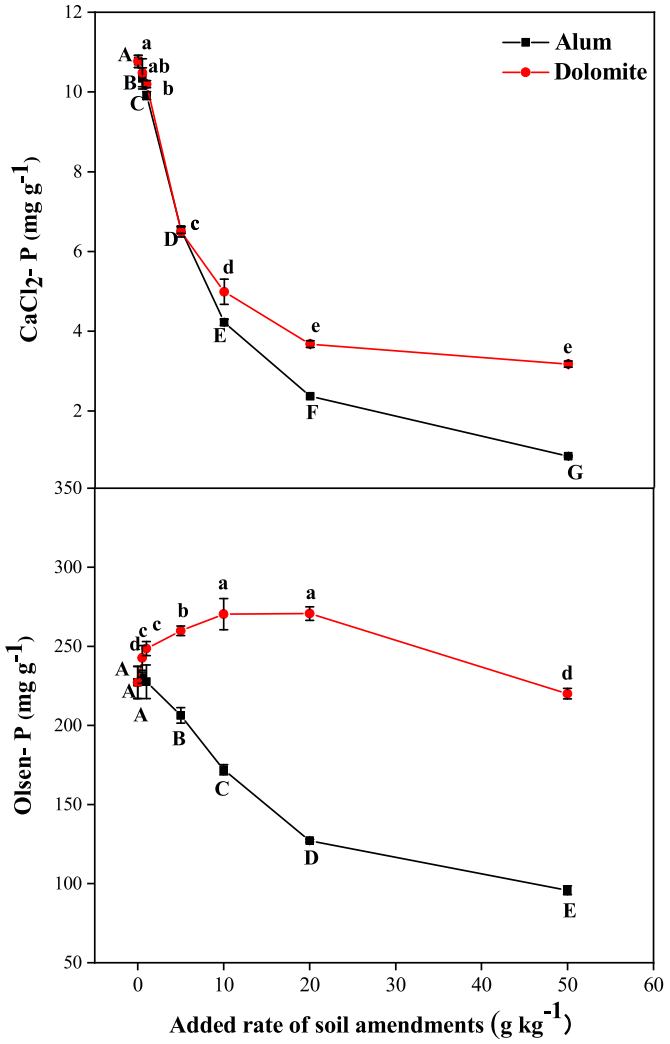

Fig. 5. Variation of $CaCl_2$—P and Olsen-P in the calcareous soil by adding 0—50 g kg^{-1} of alum or dolomite after 90 d incubation. Capital letter means the differences among the control and alum treatments, the small letter means the differences among the control and dolomite treatments. Data are the means of three replicates. Different letters in different treatments are significant at $P < 0.05$.

soil legacy P has been at very high level (Chen et al., 2019). Therefore, P sorption-desorption of the amended soil needs to be investigated as it impacts the appropriate application rate of soil amendments and P fertiliser (Wendling et al., 2013).

All the alum rates suggested an increase in the P sorbed amounts compared with control treatment (Table 2). Based on the P sorption on poorly-crystalline Al hydroxides, the formation of inner-sphere P complexes was the main mechanism to sorb P as discussed above. It was reported that P bonding capacity on poorly-crystalline Al hydroxides through bridging bidentate to form inner-sphere complexes was weaker than P precipitation (Gérard, 2016; Li et al., 2018). However, the P release showed that the use of higher rates of alum and higher P concentrations resulted in less P release, which suggested easier inner-sphere P sorption formation (Table 2). Hence, alum application rates were determined according to the degree of soil P accumulation to achieve a balance of the environmental and agricultural targets, in line with the recommendation of Zhao et al. (2018).

Dolomite amended soil treatments showed a decline of P sorbed amounts compared with the control treatment when the dolomite rates were $\leq$1 g kg^{-1} (Table 2). This was because the increase in soil pH (Supplementary Information, Table S1) resulted in the competition between —OH and P, which caused P release. However, once the dolomite rates exceed 10 g kg^{-1}, the P desorbed amounts decreased substantially (Table 2). This was identified through the P precipitation on the surface of dolomite based on P sorption mechanisms on dolomite mineral (Supplementary Information, Figs. S5c—d). Although in the present study Mg inhibited the formation of HAP and such results were backed up by the results of Salimi et al. (1985), other studies, e.g. Cao and Harris (2007) and Xu et al. (2014) have shown that Mg can also promote the formation of ACP. This can occur under high alkaline conditions due to an increase in the formation of CO_3-Mg-PO_4 bands at the carbonate sites. Therefore, weaker P adsorption on the dolomite amended soil with less P precipitation contributes to ameliorate P loss and increases P reutilisation. Dolomite addition on the calcareous soil was recommended at rates between 1 and 10 g kg^{-1} to avoid causing precipitous increase in P precipitation.

5. Conclusions

This work investigated the mechanism of P sorption on poorly-crystalline Al hydroxides and dolomite and their implication for P stabilisation in high legacy P calcareous soil. Phosphorus sorption on poorly-crystalline Al hydroxides was homogenous and the displacement of inner-sphere Al—OH groups was confirmed. Hence, the soil available P decreased while the P sorbed amounts increased in the soil amended with alum. For the dolomite, P adsorption on dolomite surface occurred at low P concentrations, but uneven P precipitated was found as a $Ca_3(PO_4)_2$ cluster at high P concentrations. However, Mg in dolomite inhibited the formation of HAP. When dolomite was added to calcareous soil, $CaCl_2$—P reduced due to the P adsorption while the Olsen-P increased when the dolomite rates were <20 g kg^{-1}. The P sorption-desorption experiments further confirmed lower P released on dolomite at higher dolomite rates and P concentration.

CRediT authorship contribution statement

Bingqian Fan: Data curation, Investigation, Methodology, Writing - original draft. **Jiahui Ding:** Software, Formal analysis, Writing - review & editing. **Owen Fenton:** Writing - review & editing, Validation. **Karen Daly:** Writing - review & editing, Visualization. **Qing Chen:** Conceptualization, Funding acquisition, Project administration, Resources, Supervision.

Acknowledgments

This work was supported by the National Key Research and Development Program of China (2016YFD0801006) and the China Agricultural Research System (CARS-23-B16).

Appendix A. Supplementary data

Supplementary data to this article can be found online at https://doi.org/10.1016/j.envpol.2020.114175.

References

Adhami, E., Maftoun, M., Ronaghi, A., Karimian, N., Yasrebi, J., Assad, M.T., 2006. Inorganic phosphorus fractionation of highly calcareous soils of Iran. Commun. Soil Sci. Plant Anal. 37, 1877—1888.

Anderson, K.R., Moore, P.A., Miller, D.M., DeLaune, P.B., Edwards, D.R., Kleinman, P.J.A., Cade-Menun, B.J., 2018. Phosphorus leaching from soil cores from a twenty-year study evaluating alum treatment of poultry litter. J. Environ. Qual. 47, 530—537.

Arai, Y., Sparks, D., 2007. Phosphate reaction dynamics in soils and soil components: a multiscale approach. Adv. Agron. 94, 135—179.

Audette, Y., O'Halloran, I.P., Evans, L.J., Voroney, R.P., 2016. Preliminary validation of a sequential fractionation method to study phosphorus chemistry in a calcareous soil. Chemosphere 152, 369–375.
Bertrand, I., Grignon, N., Hinsinger, P., Souche, G., Jaillard, B., 2001. The use of secondary ion mass spectrometry coupled with image analysis to identify and locate chemical elements in soil minerals: the example of phosphorus. Scanning 23, 279–291.
Brady, N.C., Weil, R., 2019. The nature and properties of soils. In: The Fourteenth Edition of the Original Book. Chinese Science Press.
Brennan, R.B., Fenton, O., Grant, J., Healy, M.G., 2011. Impact of chemical amendment of dairy cattle slurry on phosphorus, suspended sediment and metal loss to runoff from a grassland soil. Sci. Total Environ. 409, 5111–5118.
Cao, X., Harris, W., 2007. Carbonate and magnesium interactive effect on calcium phosphate precipitation. Environ. Sci. Technol. 42, 436–442.
Chen, S., Yan, Z., Zhang, S., Fan, B., Cade-Menun, B.J., Chen, Q., 2019. Nitrogen application favors soil organic phosphorus accumulation in calcareous vegetable fields. Biol. Fertil. Soils 55, 481–496.
Cieślik, B., Konieczka, P., 2017. A review of phosphorus recovery methods at various steps of wastewater treatment and sewage sludge management. The concept of "no solid waste generation" and analytical methods. J. Clean. Prod. 142, 1728–1740.
Cusack, P.B., Healy, M.G., Ryan, P.C., Burke, I.T., O'Donoghue, L.M., Ujaczki, É., Courtney, R., 2018. Enhancement of bauxite residue as a low-cost adsorbent for phosphorus in aqueous solution, using seawater and gypsum treatments. J. Clean. Prod. 179, 217–224.
Devau, N., Hinsinger, P., Le Cadre, E., Colomb, B., Gérard, F., 2011. Fertilization and pH effects on processes and mechanisms controlling dissolved inorganic phosphorus in soils. Geochem. Cosmochim. Acta 75, 2980–2996.
Egorova, S.R., Lamberov, A.A., 2015. Formation and distribution of phases during the dehydration of large hydrargillite floccules. Inorg. Mater. 51, 331–339.
Eslamian, F., Qi, Z., Tate, M.J., Zhang, T., Prasher, S.O., 2018. Phosphorus loss mitigation in leachate and surface runoff from clay loam soil using four lime-based materials. Water, Air, Soil Pollut. 229, 97–110.
Essington, M.E., 2015. Soil and Water Chemistry: an Integrative Approach. CRC press.
Fan, B., Wang, J., Fenton, O., Daly, K., Ezzati, G., Chen, Q., 2019. Strategic differences in phosphorus stabilization by alum and dolomite amendments in calcareous and red soils. Environ. Sci. Pollut. Res. 26, 4842–4854.
Fenton, O., Kirwan, L., Ó hUallacháin, D., Healy, M.G., 2011. The effectiveness and feasibility of using ochre as a soil amendment to sequester dissolved reactive phosphorus in runoff. Water, Air. Soil Pollut. 223, 1249–1261.
Freeman, J., Rowell, D., 1981. The adsorption and precipitation of phosphate onto calcite. J. Soil Sci. 32, 75–84.
Ganesan, K., Epple, M., 2008. Calcium phosphate nanoparticles as nuclei for the preparation of colloidal calcium phytate. New J. Chem. 32, 1326–1330.
Gérard, F., 2016. Clay minerals, iron/aluminum oxides, and their contribution to phosphate sorption in soils — a myth revisited. Geoderma 262, 213–226.
Gunasekaran, S., Anbalagan, G., Pandi, S., 2006. Raman and infrared spectra of carbonates of calcite structure. J. Raman Spectrosc. 37, 892–899.
Gustafsson, J.P., Mwamila, L.B., Kergoat, K., 2012. The pH dependence of phosphate sorption and desorption in Swedish agricultural soils. Geoderma 189–190, 304–311.
Gypser, S., Hirsch, F., Schleicher, A.M., Freese, D., 2018. Impact of crystalline and amorphous iron- and aluminum hydroxides on mechanisms of phosphate adsorption and desorption. J. Environ. Sci. 70, 175–189.
Helfenstein, J., Tamburini, F., Sperber, C.V., Massey, M.S., Pistocchi, C., Chadwick, O.A., Vitousek, P.M., Kretzschmar, R., Frossard, E., 2018. Combining spectroscopic and isotopic techniques gives a dynamic view of phosphorus cycling in soil. Nat. Commun. 9, 3226–3235.
Hinedi, Z., Goldberg, S., Chang, A., Yesinowski, J., 1992. A 31P and 1H MAS NMR study of phosphate sorption onto calcium carbonate. J. Colloid Interface Sci. 152, 141–160.
Hosni, K., Srasra, E., 2010. Evaluation of phosphate removal from water by calcined-LDH synthesized from the dolomite. Colloid J. 72, 423–431.
Huang, L., Yang, J., Xu, Y., Lei, J., Luo, X., Cade-Menun, B.J., 2018. The contrasting effects of alum-treated chicken manures and KH_2PO_4 on phosphorus behavior in soils. J. Environ. Qual. 47, 345–352.
Ippolito, J.A., Barbarick, K.A., Heil, D.M., Chandler, J.P., Redente, E.F., 2003. Phosphorus retention mechanisms of a water treatment residual. J. Environ. Qual. 32, 1857–1864.
Jiang, B., Gu, Y., 1989. A suggested fractionation scheme of inorganic phosphorus in calcareous soils. Fert. Res. 20, 159–165.
Kolesova, V.A., Ryskin, Y.I., 1959. Infrared absorption spectrum of hydrargillite $Al(OH)_3$. Optic Spectrosc. 7, 165–175.
Krumina, L., Kenney, J.P.L., Loring, J.S., Persson, P., 2016. Desorption mechanisms of phosphate from ferrihydrite and goethite surfaces. Chem. Geol. 427, 54–64.
Leng, L., Yuan, X., Zeng, G., Shao, J., Chen, X., Wu, Z., Hou, W., Xin, P., 2015. Surface characterization of rice husk bio-char produced by liquefaction and application for cationic dye (Malachite green) adsorption. Fuel 155, 77–85.
Li, H., Huang, G., Meng, Q., Ma, L., Yuan, L., Wang, F., Zhang, W., Cui, Z., Shen, J., Chen, X., 2011. Integrated soil and plant phosphorus management for crop and environment in China. A review. Plant Soil 349, 157–167.
Li, R., Wang, J.J., Zhang, Z., Awasthi, M.K., Du, D., Dang, P., Huang, Q., Zhang, Y., Wang, L., 2018. Recovery of phosphate and dissolved organic matter from aqueous solution using a novel CaO-MgO hybrid carbon composite and its feasibility in phosphorus recycling. Sci. Total Environ. 642, 526–536.
Li, R., Wang, J.J., Zhou, B., Zhang, Z., Shuai, L., Shuang, L., Ran, X., 2017. Simultaneous capture removal of phosphate, ammonium and organic substances by MgO impregnated biochar and its potential use in swine wastewater treatment. J. Clean. Prod. 147, 96–107.
Li, W., Feng, X., Yan, Y., Sparks, D.L., Phillips, B.L., 2013a. Solid-state NMR spectroscopic study of phosphate sorption mechanisms on aluminum (Hydr)oxides. Environ. Sci. Technol. 47, 8308–8315.
Li, W., Pierre-Louis, A.-M., Kwon, K.D., Kubicki, J.D., Strongin, D.R., Phillips, B.L., 2013b. Molecular level investigations of phosphate sorption on corundum (α-Al2O3) by 31P solid state NMR, ATR-FTIR and quantum chemical calculation. Geochem. Cosmochim. Acta 107, 252–266.
Liang, L.Z., Zhao, X.Q., Yi, X.Y., Chen, Z.C., Dong, X.Y., Chen, R.F., Shen, R.F., 2013. Excessive application of nitrogen and phosphorus fertilizers induces soil acidification and phosphorus enrichment during vegetable production in Yangtze River Delta, China. Soil Use Manag. 29, 161–168.
Lookman, R., Grobet, P., Merckx, R., Riemsdijk, W.H.V., 1997. Application of 31P and 27Al MAS NMR for phosphate speciation studies in soil and aluminium hydroxides: promises and constraints. Geoderma 80, 369–388.
Lookman, R., Grobet, P., Merckx, R., Vlassak, K., 1994. Phosphate sorption by synthetic amorphous aluminum hydroxides: a 27Al and 31P solid-state MAS NMR spectroscopy study. Eur. J. Soil Sci. 45, 37–44.
Makris, K.C., Harris, W.G., O'Connor, G.A., Obreza, T.A., 2004. Phosphorus immobilization in micropores of drinking-water treatment residuals: implications for long-term stability. Environ. Sci. Technol. 38, 6590–6596.
Mekonnen, M.M., Hoekstra, A.Y., 2018. Global anthropogenic phosphorus loads to freshwater and associated grey water footprints and water pollution levels: a high-resolution global study. Water Resour. Res. 54, 345–358.
Miyittah, M.K., Stanley, C.D., Mackowiak, C., Rhue, D.R., Rechcigl, J.E., 2011. Developing a remediation strategy for phosphorus immobilization: effect of co-blending, Al-residual and Ca-Mg amendments in a manure-impacted spodosol. Soil Sediment Contam. 20, 337–352.
Murphy, J., Riley, J.P., 1962. A modified single solution method for the determination of phosphate in natural waters. Anal. Chim. Acta 27, 31–36.
Murrmann, R.P., Peech, M., 1969. Effect of pH on labile and soluble phosphate in soils. Soil Sci. Soc. Am. J. 33, 205–210.
Myronyuk, I.F., Mandzyuk, V.I., Sachko, V.M., Gun'Ko, V.M., 2016. Structural and morphological features of disperse alumina synthesized using aluminum nitrate nonahydrate. Nanoscale Res. Lett. 11, 153–161.
Novak, J.M., Watts, D.W., 2005. An alum-based water treatment residual can reduce extractable phosphorus concentrations in three phosphorus-enriched coastal plain soils. J. Environ. Qual. 34, 1820–1827.
O' Flynn, C.J., Fenton, O., Wall, D., Brennan, R.B., McLaughlin, M.J., Healy, M.G., Nicholson, F., 2018. Influence of soil phosphorus status, texture, pH and metal content on the efficacy of amendments to pig slurry in reducing phosphorus losses. Soil Use Manag. 34, 1–8.
Olsen, S.R., 1954. Estimation of available phosphorus in soils by extraction with sodium bicarbonate. USDA Circular 939, 1–19.
Pautler, M.C., Sims, J.T., 2000. Relationships between soil test phosphorus, soluble phosphorus, and phosphorus saturation in Delaware soils. Soil Sci. Soc. Am. J. 64, 765–773.
Powers, S.M., Bruulsema, T.W., Burt, T.P., Chan, N.I., Elser, J.J., Haygarth, P.M., Howden, N.J.K., Jarvie, H.P., Lyu, Y., Peterson, H.M., Sharpley, Andrew N., Shen, J., Worrall, F., Zhang, F., 2016. Long-term accumulation and transport of anthropogenic phosphorus in three river basins. Nat. Geosci. 9, 353–356.
Rajan, S.S.S., Perrott, K.W., Saunders, W.M.H., 1974. Identification of phosphate-reactive sites of hydrous alumina from proton consumption during phosphate adsorption at constant pH values. J. Soil Sci. 25, 438–447.
Ruan, H.D., Frost, R.L., Kloprogge, J.T., 2001. Comparison of Raman spectra in characterizing gibbsite, bayerite, diaspore and boehmite. J. Raman Spectrosc. 32, 745–750.
Rydin, E., 2000. Potentially mobile phosphorus in Lake Erken sediment. Water Res. 34, 2037–2042.
Salimi, M., Heughebaert, J., Nancollas, G., 1985. Crystal growth of calcium phosphates in the presence of magnesium ions. Langmuir 1, 119–122.
Schofield, R., 1955. Can a precise meaning be given to 'available'soil phosphorus. Soils Fert. 18, 373–375.
Shang, C., Stewart, J.W.B., Huang, P.M., 1992. pH effect on kinetics of adsorption of organic and inorganic phosphates by short-range ordered aluminum and iron precipitates. Geoderma 53, 1–14.
Ślósarczyk, A., Paszkiewicz, Z., Paluszkiewicz, C., 2005. FTIR and XRD evaluation of carbonated hydroxyapatite powders synthesized by wet methods. J. Mol. Struct. 744, 657–661.
Sujana, M.G., Soma, G., Vasumathi, N., Anand, S., 2009. Studies on fluoride adsorption capacities of amorphous Fe/Al mixed hydroxides from aqueous solutions. J. Fluor. Chem. 130, 749–754.
Wan, B., Huang, R., Diaz, J.M., Tang, Y., 2019. Polyphosphate adsorption and hydrolysis on aluminum oxides. Environ. Sci. Technol. 53, 9542–9552.
Wan, B., Yan, Y., Liu, F., Tan, W., Chen, X., Feng, X., 2016. Surface adsorption and precipitation of inositol hexakisphosphate on calcite: a comparison with orthophosphate. Chem. Geol. 421, 103–111.
Wang, X., Phillips, B., Boily, J.-F., Hu, Y., Hu, Z., Yang, P., Feng, X., Xu, W., Zhu, M., 2019. Phosphate sorption speciation and precipitation mechanisms on amorphous aluminum hydroxide. Soil Syst. 3, 1–17.
Wendling, L.A., Blomberg, P., Sarlin, T., Priha, O., Arnold, M., 2013. Phosphorus

sorption and recovery using mineral-based materials: sorption mechanisms and potential phytoavailability. Appl. Geochem. 37, 157–169.
Xu, N., Yin, H., Chen, Z., Liu, S., Chen, M., Zhang, J., 2014. Mechanisms of phosphate retention by calcite: effects of magnesium and pH. J. Soils Sediments 14, 495–503.
Yuan, X., Xia, W., An, J., Yin, J., Zhou, X., Yang, W., 2015. Kinetic and thermodynamic studies on the phosphate adsorption removal by dolomite mineral. J. Chem. 2015, 1–8.
Zak, D., Gelbrecht, J., Steinberg, C.E.W., 2004. Phosphorus retention at the redox interface of peatlands adjacent to surface waters in northeast Germany. Biogeochemistry 70, 357–368.
Zhao, Y., Liu, R., Awe, O.W., Yang, Y., Shen, C., 2018. Acceptability of land application of alum-based water treatment residuals – an explicit and comprehensive review. Chem. Eng. J. 353, 717–726.
Zhou, J., Yang, S., Yu, J., 2011. Facile fabrication of mesoporous MgO microspheres and their enhanced adsorption performance for phosphate from aqueous solutions. Colloid. Surface. 379, 102–108.
Zhou, M., Liu, X., Meng, Q., Zeng, X., Zhang, J., Li, D., Wang, J., Du, W., Ma, X., 2019. Additional application of aluminum sulfate with different fertilizers ameliorates saline-sodic soil of Songnen Plain in Northeast China. J. Soils Sediments 19, 3521–3533.